Jingfei Yin
Key Laboratory for Precision and Non-Traditional Machining Technology of Ministry of Education,
Dalian University of Technology,
No. 2, Linggong Road,
Dalian, Liaoning 116024, China
e-mail: jingfei_yin@mail.dlut.edu.cn

Qian Bai
Key Laboratory for Precision and Non-Traditional Machining Technology of Ministry of Education,
Dalian University of Technology,
No. 2, Linggong Road,
Dalian, Liaoning 116024, China
e-mail: baiqian@dlut.edu.cn

Bi Zhang[1]
Fellow ASME
College of Engineering,
Southern University of Science and Technology,
No. 1088, Xueyuan Boulevard,
Shenzhen, Guangdong 518055, China
e-mail: zhangb@sustech.edu.cn

Subsurface Damage Detection on Ground Silicon Wafers Using Polarized Laser Scattering

A silicon wafer is important for the electronic and computer industries. However, subsurface damage (SSD), which is detrimental to the performance and lifetime of a silicon chip, is easily induced in a silicon wafer during a grinding process since silicon is typically a hard and brittle material. Therefore, it is necessary to detect and remove SSD in the subsequent processes. In this study, a polarized laser scattering (PLS) system is installed to detect the SSD in a ground wafer. It is found that not only the subsurface crack but also the residual stress leads to depolarization of an incident light. The effects of residual stress on depolarization are studied. The residual stress results in the photoelasticity, which causes the depolarization of the incident light in the PLS system. The depolarization caused by the residual stress is determined by the directions and the difference of the principal stresses. When the polarization direction of the incident light is aligned with one of the principal stresses, the effects of the residual stress can be minimized; therefore, the subsurface crack can be quantitatively estimated by PLS. [DOI: 10.1115/1.4044417]

Keywords: silicon wafer, subsurface damage, residual stress, laser scattering, depolarization

1 Introduction

Single crystal silicon is widely used as a substrate material in the semiconductor industry because of the excellent physical and electronic properties [1–9]. A silicon wafer is hard and brittle, which makes it hard to machine. Grinding is the most efficient process to machine the silicon wafer [10,11]. However, subsurface damage (SSD), including subsurface cracks (SSCs) and residual stresses (RSs), is inevitably induced in a grinding process [1–3,12]. SSD, especially SSC, degrades the performance and reduces the life of the final products. Therefore, it is necessary to detect and remove SSD by the subsequent processes.

Traditionally, many methods can be used to detect SSD. The destructive methods, such as taper polishing [10,13,14], magnetorheological polishing [15], cross-sectional microscopy [6,16,17], transmission electron microscopy [3,12,18], are reliable and easy to operate, but they are time consuming [19]. The nondestructive methods, including the photoelastic inspection techniques [20–24], Raman microspectroscopy [25–28], acoustic microscopy [29,30], and laser scattering [4,31–35], preserve the part and are more efficient. By using the photoelastic inspection techniques to detect SSD, many studies have been devoted to the relationship between the measured signals and the stresses induced by the four-point bending [20] or the three-point bending [36] methods. The scanning infrared depolarization technique, one of the photoelastic inspection techniques, was applied to monitor SSD induced in different processes [22,23]. The photoelastic inspection techniques are generally applied to detect residual stresses, but cannot quantitatively detect SSC. Although Raman microspectroscopy is used to detect the residual stresses and phase transformation in a ground surface, it is limited to the small detection area. The acoustic microscopy can be applied to detect the whole surface of a part with a considerably high efficiency, but the detection signal is easily mixed with the surface roughness-induced signal [37], which compromises the detection accuracy. Some laser scattering methods also suffer from the surface scattering due to surface roughness [31,32,35]. Exceptionally, the polarized laser scattering (PLS) method can be used to directly detect the SSC beneath a rough surface, since surface roughness has little effect on detection [38]. Therefore, the PLS method is promising for the detection of SSD in a ground silicon wafer.

In the PLS method, SSD can be estimated by the intensity of the depolarized light in the emergent light with respect to the incident light. RS and SSC lead to depolarization of the emergent light in different mechanisms: RS induces photoelasticity, while SSC induces multiscattering. Schematics of the depolarization caused by SSC are shown in Fig. 1(*a*). (i) The incident light irradiates the surface of the silicon wafer and is scattered by the surface. The polarization of the light is the same as that of the incident light. (ii) The light penetrates the silicon wafer. The transmission light is multiscattered by SSC, which changes the polarization of the light. (iii) The emergent light including the surface scattering light exits the wafer and is partially polarized. Schematics of the depolarization caused by the residual stress are shown in Fig. 1(*b*). (i) The incident light irradiates the surface subjected to residual stress. The two principal stresses are σ_1 and σ_2. θ is the angle between the polarization plane of the incident light and the first principal stress. (ii) The light decomposes into two linear polarized lights along the directions of the principal stresses in the wafer due to photoelasticity. The two lights travel in different velocities in the wafer when the levels of the two principal stresses are different, which results in a phase retardation when they exit the wafer [39]. (iii) The emergent light combining the two linear polarized lights is depolarized.

During a grinding process, residual stresses are simultaneously induced and accompanied by SSC in a wafer. In the detection of SSD using the PLS method, the effects of residual stresses were neglected in the previous studies [4,33,34,40]. However, the grinding-induced residual stresses are asymmetrically distributed in the wafer [2,12], i.e., the levels of the two principal stresses are different. On the basis of Fig. 1(*b*), RS leads to photoelasticity, which results in the depolarization of the emergent light, and thus influences the detection results of the PLS method. Therefore, the coupling effect between SSC and RS needs to be considered in the application of the PLS method to a ground silicon wafer.

In this study, the PLS system is used to detect SSD in the ground silicon wafers. The study focuses on the effect of residual stresses on the detection of SSD in a wafer. RS influences the detection

[1]Corresponding author.

Manuscript received August 31, 2018; final manuscript received July 26, 2019; published online August 2, 2019. Assoc. Editor: Laine Mears.

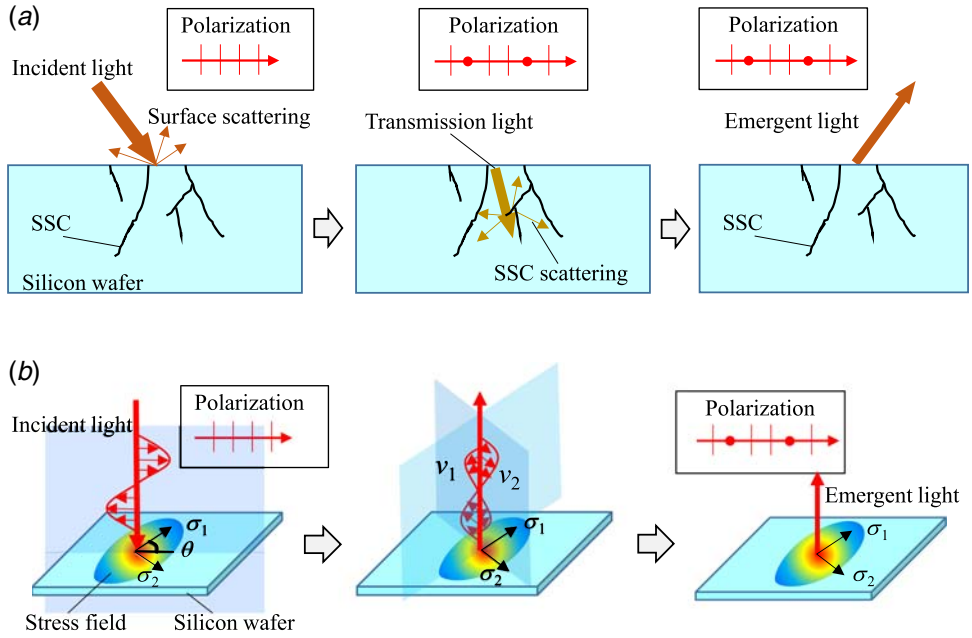

Fig. 1 Schematics of the depolarization of light in the PLS detection. (*a*) Schematics of the depolarization caused by SSC: (i) surface scattering and the polarization reserves; (ii) transmission light is scattered by SSC and the depolarization takes place; and (iii) emergent light is partially polarized. (*b*) Schematics of the depolarization caused by RS: (i) linearly polarized light irradiating the surface; (ii) light decomposed into two branches along the directions of the first and second principal stresses; and (iii) emergent light is partially polarized.

regardless of the size of the abrasive grains that are used to grind the silicon wafer.

2 Experimental Methodology

2.1 Setup of Polarized Laser Scattering System. Figure 2 shows the configuration of the PLS system. A continuous wave solid-state laser emits an incident light of a wavelength of 914 nm. The light is linearly polarized after going through a polarizer with an extinction ratio of 100. Then, the light goes through a polarized beam splitter (PBS) with an extinction ratio of 3000 and is reflected by a reflector. Finally, the light is focused on the surface of a wafer by the lens. A part of the light is scattered by the rough surface, and the other part penetrates the wafer and is scattered by SSD. The transmission light is partially cross-polarized after it interacts with SSD. The scattered light, including the light with the original polarized direction and the light with the cross-polarized direction, is captured by the lens and reflected by the reflector. The cross-polarized light consisting of the SSD information is reflected by PBS. As a filter, the Glan polarizer ensures that the light going into the detector is purely cross-polarized light. Then, the cross-polarized light is detected with a detector that transfers the light signal into a voltage signal. The detection signal is acquired with a data acquisition device. The wafer was placed on a translation stage, which provided the scanning along the radius of the wafer.

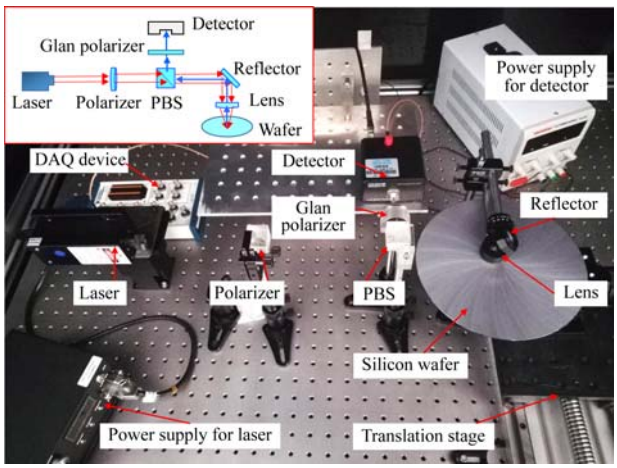

Fig. 2 The configuration of the PLS detection system. The inset figure shows the schematics of the light path.

2.2 Sample Preparation. A commercial wafer-grinding machine (Okamoto VG401 MK II), as shown in Fig. 3, was used to grind silicon wafers. In the grinding process, a wafer was fixed on the vacuum chuck of the worktable. A cup-type grinding wheel was mounted to the spindle of the machine. During the grinding process, the rotational direction of the worktable was the same as that of the wheel. Material removal mainly depended on the rotation and axial feed motion of the wheel. The wafer was cooled with the deionized water and was monitored for its thickness change with an in-process thickness measurement device. In the study, one 2-in. polished wafer and three 8-in. ground (100) silicon wafers were used in PLS detection. One of the 8-in. wafers was ground by a diamond wheel of mesh size #400, the second one by a diamond wheel of mesh size #600, and the third one by a diamond wheel of mesh size #20,000. Grinding parameters are listed in Table 1. The coolant used in grinding was deionized water.

2.3 Stress Measurement. In order to study the stress effect on the detection with the PLS system, a polished 2-in. silicon wafer (001) with a thickness of 400 μm was used, eliminating the influence of the grinding-induced cracks. The process of stress measurement is shown in Fig. 4. The wafer was elastically deformed on a device by a pushing rod. Then, an area of 25×20 mm in the deformed wafer was raster scanned by a surface measurement probe (TALOR HOBSON PGI 840). The surface contour of the

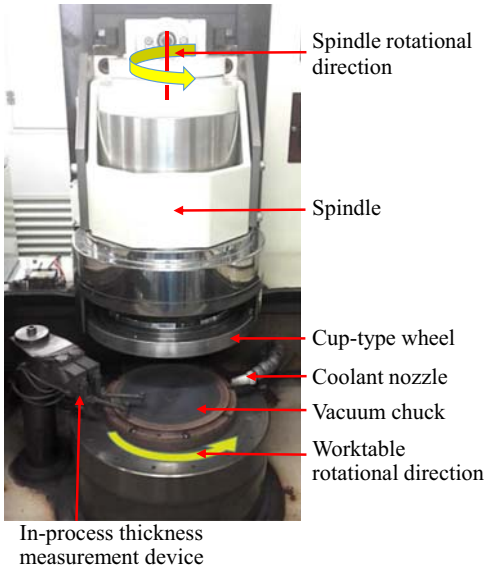

Fig. 3 The experimental setup for silicon wafer grinding

Table 1 Grinding parameters for the silicon wafers

Grinding wheel	Spindle speed (rpm)	Worktable speed (rpm)	Axial feed rate (μm/min)	Spark-out duration (s)
#400	2399	120	90	10
#600	2399	120	90	10
#20,000	2399	120	3	10

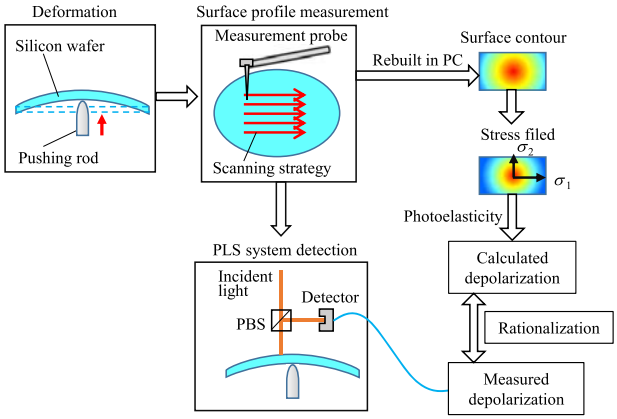

Fig. 4 The process of the stress measurement

scanned area was rebuilt with MATLAB. On the basis of rebuilt contour, principal stresses in the wafer were determined, and the depolarization was thus calculated. In this study, a depolarization coefficient was defined as the ratio of the depolarized light intensity to the incident light intensity to reflect the level of depolarization caused by stresses. On the other hand, the deformed wafer was detected with the PLS system, and thus, the depolarization caused by stress can be measured. By comparing the calculated depolarization coefficient with the measured depolarization signal, the relationship between the principal stresses and the light intensity from the PLS system was rationalized.

A schematic view of the device for deforming a silicon wafer is shown in Fig. 5(*a*). The pushing rod was driven upward to cause the silicon wafer to deform. Different displacements of the pushing rod caused different elastic deformation of the silicon wafer, i.e., the

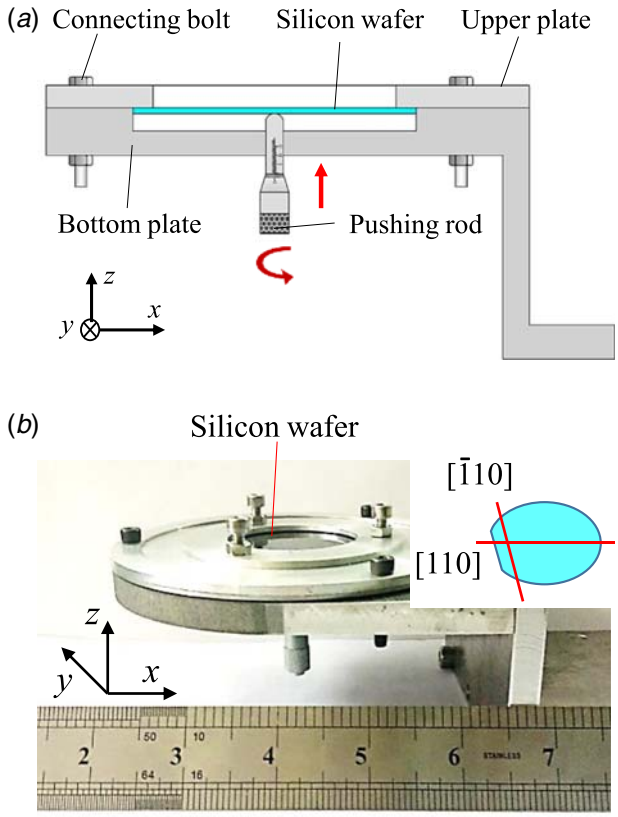

Fig. 5 The device for deforming the silicon wafer: (*a*) schematic view of the device and (*b*) photographic view of the device

wafer was subjected to different stresses at different displacements. Figure 5(*b*) shows a photographic view of the device and the crystal orientation of the fixed silicon wafer. The x and y axes were aligned with the $\langle 110 \rangle$ orientation, and the z axis was aligned with the [001] orientation.

On the basis of the elasticity theory, the two principal curvatures at the point of interest can be calculated [12]:

$$\begin{cases} \kappa_1 = \kappa_m + \kappa_a \\ \kappa_2 = \kappa_m - \kappa_a \\ \theta = \cos^{-1}\left[\dfrac{(\kappa_0 + \kappa_m)}{\kappa_a}\right] \end{cases} \tag{1}$$

with

$$\begin{cases} \kappa_m = \dfrac{(\kappa_0 + \kappa_{90})}{2} \\ \kappa_a = [(\kappa_0 - \kappa_m)^2 + (\kappa_m - \kappa_{45})^2]^{1/2} \end{cases} \tag{2}$$

where κ_0, κ_{45}, and κ_{90} are the curvatures in the directions of 0 deg, 45 deg, and 90 deg with respect to x axis, respectively. Stresses are computed based on curvatures as given in Eq. (3):

$$\sigma = E \cdot t \cdot \kappa \tag{3}$$

where E is the elastic modulus of the silicon wafer ($E = 160$ GPa) and t is the thickness of the wafer.

On the basis of photoelasticity theory, the depolarization coefficient is obtained as follows:

$$\frac{I}{I_i} = D(\theta) \cdot D(\Delta\sigma) = \sin^2(2\theta) \cdot \sin^2\left(\frac{\varphi}{2}\right) \tag{4}$$

where I is the depolarized light intensity; I_i is the incident light intensity, which is constant for a given laser power; $D(\theta)$ and $D(\Delta\sigma)$ are defined as an angle-related coefficient and a stress-related

coefficient, respectively; θ is the angle between the polarization plane of the incident light and the first principal stress in the silicon wafer; and φ is the phase retardation [41], which is given as follows:

$$\varphi = k \cdot \Delta\sigma = \frac{2\pi C \cdot d}{\lambda}(\sigma_1 - \sigma_2) \tag{5}$$

where C is the stress-optic coefficient of silicon and varies in different orientations. However, different studies concluded different results [20,36,42], generally in a range of 1.4×10^{-11} to 3×10^{-11} Pa^{-1}. In this paper, C is chosen as 1.6×10^{-11} Pa^{-1}; d is the distance that light goes into the silicon wafer and equals to two times the detected depth. For the silicon wafer, d is approximately 400 μm based on the optical transmission property at the light wavelength of 914 nm [38]. λ is the wavelength of the incident light and σ_1 and σ_2 are the first and second principal stresses, respectively.

In this study, a fixed point on the surface of the deformed wafer was chosen as the detection point. The point was subjected to different stress conditions induced by the different deformations of the wafer.

2.4 Subsurface Damage Detection. The wafers ground with the #400 and #600 wheels, in which both SSC and RS co-exist, were measured with the PLS system to study the coupling effect of SSC and RS. Each ground wafer was measured along the [100] and [110] orientations, as shown in Fig. 6, where dashed lines represent the measurement trajectory, l represents one of the grinding marks, and ϕ is the angle of the grinding mark with respect to the measurement trajectory. SSC in the two ground wafers was detected with the cross-sectional microscopy. The samples for SSC detection were cut along the radial direction and numbered A, B, C, and D.

The wafer ground with the #20,000 wheel was also measured with the PLS system to study the effect of the RS excluding the influence of SSC. It was measured along the radial direction with an elevated incident laser power. The SSD in the #20,000 wheel ground wafer was inspected with a transmission electron microscope (TEM).

3 Results and Discussion

Figures 7(*a*)–7(*e*) show the contours of the deformed surface of the polished wafer, which were rebuilt with MATLAB. The detection point is marked as P in the figures. As shown in Fig. 7(*f*), the deflection of the deformed wafer obviously increases with the displacement of the pushing rod, and the difference of the principal stresses $\Delta\sigma$ also increases. Based on $\Delta\sigma$, the depolarization coefficient was obtained by Eqs. (4) and (5), and its variation is compared with that of the depolarization signal measured with the PLS system, as shown in Fig. 8. The variation tendency of the depolarization coefficient is consistent with that of the depolarization signal, which indicates that the photoelasticity occurs in the detection with the PLS system. When the deformed wafer was transferred from the PLS system to the surface measurement device, the stresses in the wafer might have been partially relieved. As a result, the tendency of the depolarization coefficient is shifted to the right compared with that of the depolarization signal.

Moreover, Fig. 8 shows a drastic increase in the depolarization signal when the displacement of the pushing rod is larger than 0.6 mm. It can be deduced that a larger stress results in more depolarization, which might be due to the fact that the stresses change the lattice spacings of the silicon wafer. In a stress-free wafer, different crystal orientations, i.e., different lattice spacings, lead to varied stress-optic coefficients [20]. In other words, the depolarization signal measured with the PLS system might be related to a change in the lattice spacing of the wafer caused by stress.

Figures 9(*a*) and 9(*b*) show the radial distribution of the depolarization signal over the ground surfaces. The signal has a similar distribution along both the [110] and [100] crystal orientations. The signal of the wafer surface ground with the #400 wheel is larger than that of the wafer surface ground with the #600 wheel. The main reason could be that the larger abrasive grains might have induced larger subsurface cracks, which results in more depolarization of the incident light [34] from scattering by the walls of SSC.

Additionally, the signal is unevenly distributed along the radial direction on the ground surfaces, as shown in Fig. 9. The reason for the fluctuation is discussed as follows. Generally, a larger SSC leads to a larger depolarization signal. Besides SSC, the residual stress can also affect the detected signal by leading to photoelasticity. In the study, the wafers endured the spark-out grinding process. Figure 10 shows the radial distribution of the depth of SSC of the wafers ground with the #400 wheel and the #600 wheel. The depth of SSC is uniform along the radius of the wafers, which coincides with the results obtained in Gao et al.'s study [43]. Since the depth of SSC is uniformly distributed along the radial direction in the wafer after the spark-out process, as shown in Fig. 10, the signal caused by SSC should be uniform along the radial direction of the wafer. Therefore, the effect of

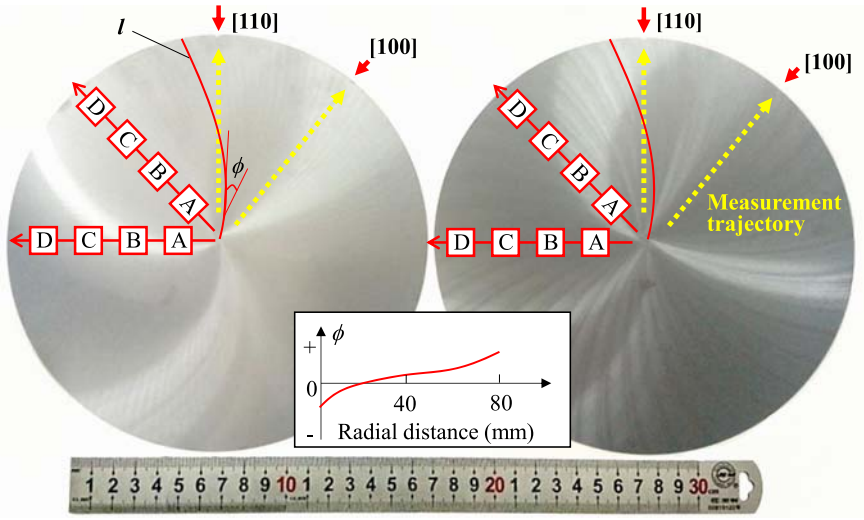

Fig. 6 The silicon wafer ground by #400 wheel (left) and #600 wheel (right). The inset shows the variation of the angle of the grinding mark with respect to the measurement trajectory.

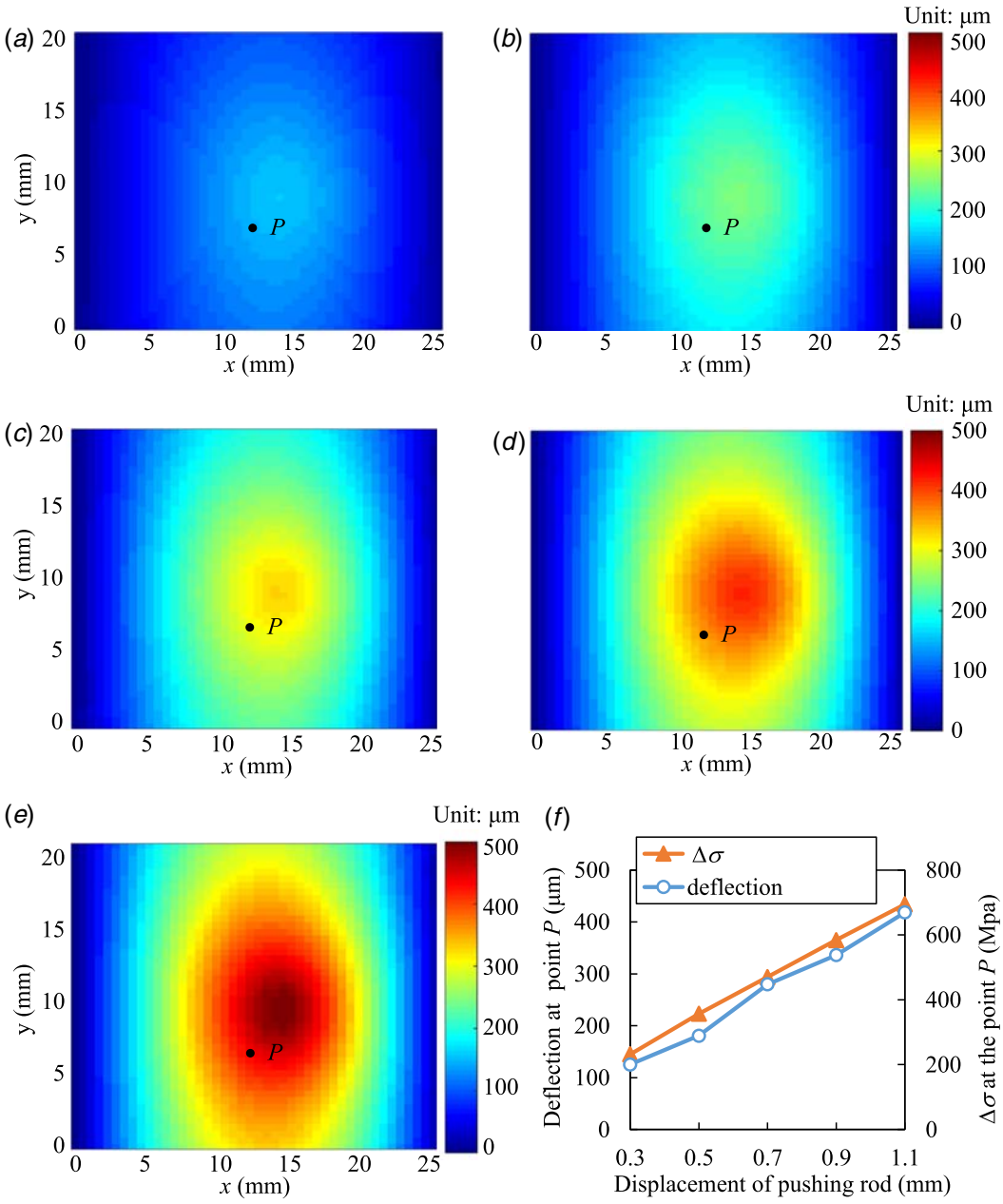

Fig. 7 Contours of the deformed wafer at various displacements. (*a*)–(e) Contours at the displacements of 0.3 mm, 0.5 mm, 0.7 mm, 0.9 mm, and 1.1 mm, respectively. (*f*) Deflection and principal stresses at point *P* varying with the displacement of the pushing rod.

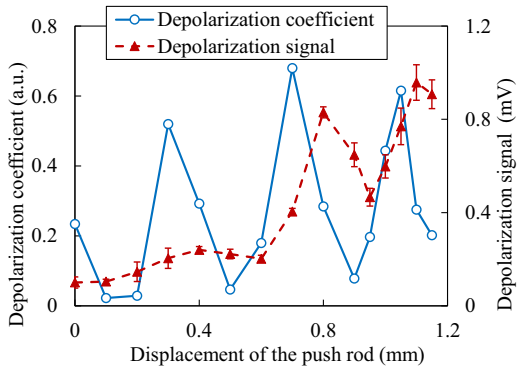

Fig. 8 The depolarization coefficient and the depolarization signal at different displacements of the pushing rod

SSC on the fluctuation of the detection signal is excluded. The cause of the fluctuation should be the residual stress. In the ground wafers, the residual stress varies along the radial direction, which causes a fluctuation in the detection signal.

The deviation of the depolarization signal in the radial intervals along the measurement trajectory is shown in Fig. 11. At the range of 10–20 mm, the deviation is smaller than that within the adjacent intervals. As shown in Eq. (4), the depolarization caused by the photoelasticity depends not only on the difference of the principal stresses but also on the angle between the direction of the principal stresses and the polarization direction of the incident light. The directions of the principal stresses have been found to align with the grinding marks. As shown in Fig. 6, from the center to the edge, the angle of the grinding marks with respect to the measurement trajectory increases from negative to positive. At the range of 10–20 mm, the directions of the grinding marks are nearly parallel to the measurement trajectory, i.e., θ is close to

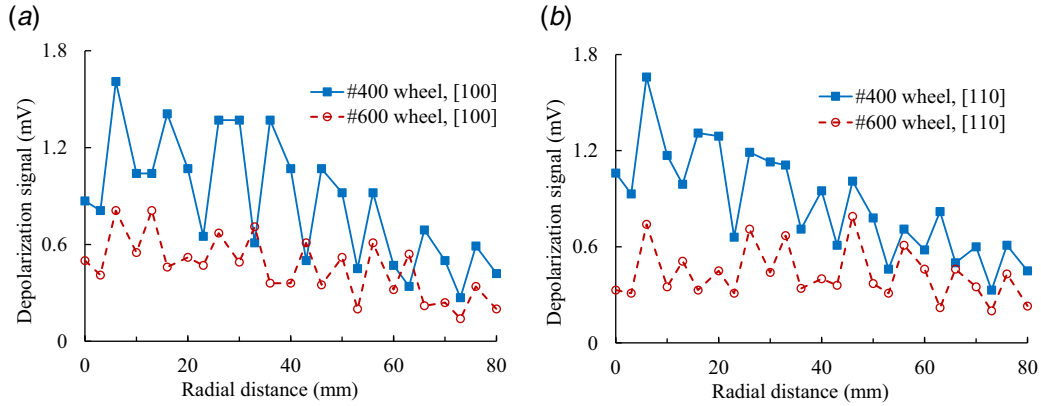

Fig. 9 The radial distribution of the depolarization signals: (*a*) along the [100] orientation and (*b*) along the [110] orientation of the ground wafers

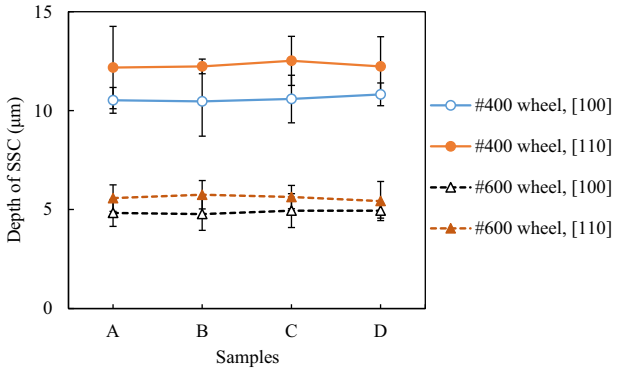

Fig. 10 The radial distribution of the depth of SSC in the wafers ground with the #400 wheel and the #600 wheel

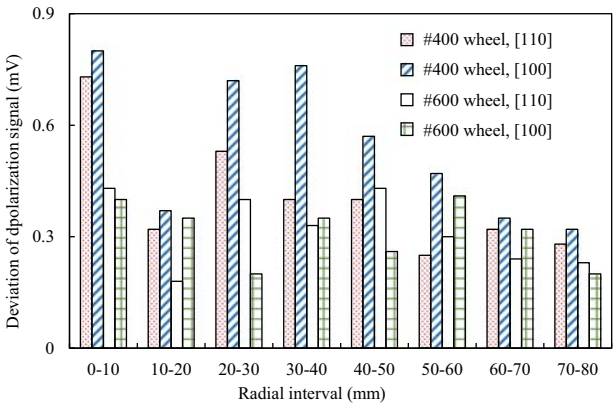

Fig. 11 Deviation of the depolarization signal along the radial direction of the wafers ground with the #400 wheel and the #600 wheel

zero, which minimizes the effect of the residual stresses. Therefore, the depolarization mainly results from the SSC scattering, and correspondingly, the deviation of the depolarization signal at the range of 10–20 mm is smaller than that within the adjacent intervals.

The deviation of the depolarization signal obtained with the #400 wheel was larger than with the #600 wheel at approximately the same position of the wafers. It can be inferred that the variation in the principal stresses is larger in the wafer ground with the #400 wheel than that with the #600 wheel.

Figure 12 shows the distribution of the depolarization signal of the wafer surface ground with the #20,000 wheel. The signal

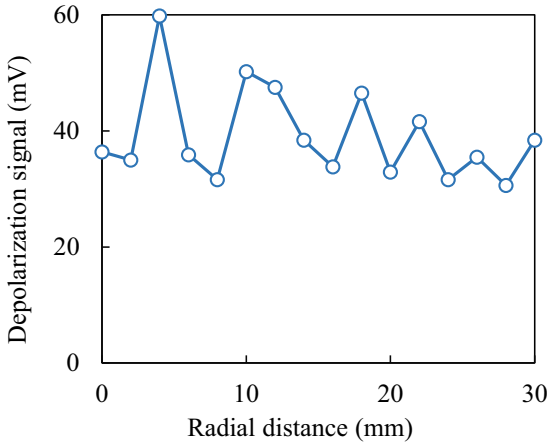

Fig. 12 Distribution of the depolarization signal of the wafer ground with the #20,000 wheel

distribution is fairly nonuniform. Generally, the grinding-induced SSC is mainly determined by the abrasive grain size [16], and it vanishes when the mesh size of the grinding wheel is over 3000 [2,44]. The TEM image of the SSD in the wafer ground with the #20,000 wheel is shown in Fig. 13. At the top of the grinding surface is an amorphous layer due to the high pressure and temperature during the grinding. Beneath the amorphous layer, several dislocations appear, which are indicated with the arrows in Fig. 13(*b*). No visible subsurface cracks exist in the wafer ground with the #20,000 wheel. Thus, the influence of SSC could be excluded in the #20,000 wheel ground wafer in this study. Therefore, the nonuniformly distributed depolarization signal of the #20,000 wheel ground wafer in Fig. 12 is considered as a result of the residual stresses due to the phase transformation at the top surface, i.e., the amorphous and dislocation layers.

4 Conclusions

The effects of residual stress are taken into consideration to detect subsurface damage in a ground silicon wafer using the polarized laser scattering method. Both the direction and the variation in the principal stresses contribute to the depolarization of the incident light. When the polarization direction of the incident light is aligned with one of the directions of the principal stresses, the effects of residual stress on the detection of SSD could be eliminated. Coincidentally, the principal stresses are aligned with the grinding marks. Therefore, it is feasible to realize the quantitative detection of the subsurface cracks by aligning the polarization direction of the

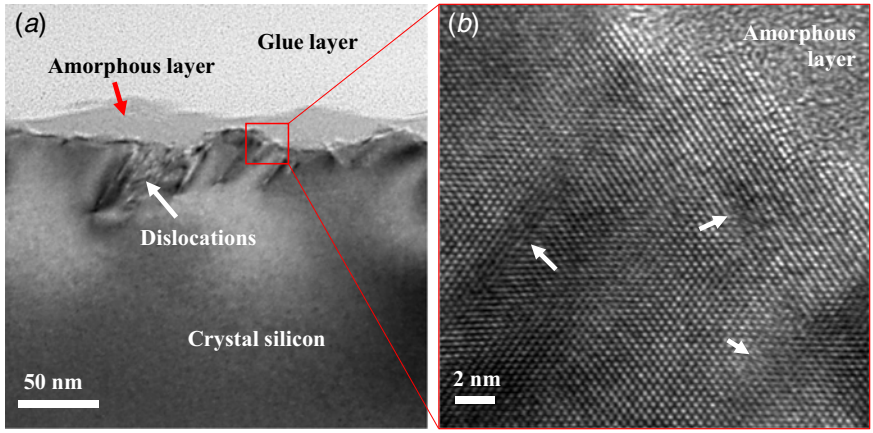

Fig. 13 TEM images of the wafer ground with the #20,000 wheel: (*a*) TEM image of the cross section of the wafer and (*b*) a high-resolution image of the selected area in (*a*). Dislocations are indicated with white arrows.

incident light with the grinding marks, which will be a topic for the future study.

Acknowledgment

This study was financially supported by the National Natural Science Foundation of China (NSFC) (Grant Nos. 51575084 and 51605077; Funder ID: 10.13039/501100001809) and the Peacock Program of Shenzhen (KQJSCX20180322152221965). The authors gratefully thank Professor Huizong Lu for his guidance in the installation of the PLS system. They also thank Associate Professor Ping Zhou for his help in the experimental design for stress measurements.

References

[1] Pei, Z. J., Billingsley, S. R., and Miura, S., 1999, "Grinding Induced Subsurface Cracks in Silicon Wafers," Int. J. Mach. Tools Manuf., **39**(7), pp. 1103–1116.
[2] Zhou, P., Xu, S., Wang, Z., Yan, Y., Kang, R., and Guo, D., 2016, "A Load Identification Method for the Grinding Damage Induced Stress (GDIS) Distribution in Silicon Wafers," Int. J. Mach. Tools Manuf., **107**(Aug.), pp. 1–7.
[3] Dong, Z., Gao, S., Huang, H., Kang, R., and Wang, Z., 2016, "Surface Integrity and Removal Mechanism of Chemical Mechanical Grinding of Silicon Wafers Using a Newly Developed Wheel," Int. J. Adv. Manuf. Technol., **83**(5–8), pp. 1231–1239.
[4] Zhang, J. M., Sun, J. G., and Pei, Z. J., 2003, "Application of Laser Scattering on Detection of Subsurface Damage in Silicon Wafers," ASME 2003 International Mechanical Engineering Congress and Exposition, Washington, DC, Nov. 15–21, pp. 15–24.
[5] Sun, J., Chen, P., Qin, F., An, T., Yu, H., and He, B., 2018, "Modelling and Experimental Study of Roughness in Silicon Wafer Self-Rotating Grinding," Precis. Eng., **51**(Jan.), pp. 625–637.
[6] Sun, J., Qin, F., Chen, P., and An, T., 2016, "A Predictive Model of Grinding Force in Silicon Wafer Self-Rotating Grinding," Int. J. Mach. Tools Manuf., **109**(Oct.), pp. 74–86.
[7] Gao, S., Kang, R., Dong, Z., and Zhang, B., 2013, "Edge Chipping of Silicon Wafers in Diamond Grinding," Int. J. Mach. Tools Manuf., **64**(Jan.), pp. 31–37.
[8] Cai, M. B., Li, X. P., and Rahman, M., 2007, "Study of the Mechanism of Nanoscale Ductile Mode Cutting of Silicon Using Molecular Dynamics Simulation," Int. J. Mach. Tools Manuf., **47**(1), pp. 75–80.
[9] Mukaida, M., and Yan, J., 2017, "Ductile Machining of Single-Crystal Silicon for Microlens Arrays by Ultraprecision Diamond Turning Using a Slow Tool Servo," Int. J. Mach. Tools Manuf., **115**(Apr.), pp. 2–14.
[10] Gao, S., Dong, Z., Kang, R., Zhang, B., and Guo, D., 2015, "Warping of Silicon Wafers Subjected to Back-Grinding Process," Precis. Eng., **40**(Apr.), pp. 87–93.
[11] Pei, Z. J., Fisher, G. R., and Liu, J., 2008, "Grinding of Silicon Wafers: A Review From Historical Perspectives," Int. J. Mach. Tools Manuf., **48**(12–13), pp. 1297–1307.
[12] Zhou, P., Yan, Y., Huang, N., Wang, Z., Kang, R., and Guo, D., 2017, "Residual Stress Distribution in Silicon Wafers Machined by Rotational Grinding," ASME J. Manuf. Sci. Eng., **139**(8), p. 081012.
[13] Esmaeilzare, A., Rahimi, A., and Rezaei, S. M., 2014, "Investigation of Subsurface Damages and Surface Roughness in Grinding Process of Zerodur® Glass–Ceramic," Appl. Surf. Sci., **313**(Sept.), pp. 67–75.
[14] Gao, R., Wang, H., Wang, C., Feng, S., and Zhu, B., 2017, "Characterization Methods of Subsurface Cracks in Grinding of Optical Elements," IOP Conf. Ser. Mater. Sci. Eng., **250**(1), p. 12025.
[15] Li, S., Wang, Z., and Wu, Y., 2008, "Relationship Between Subsurface Damage and Surface Roughness of Optical Materials in Grinding and Lapping Processes," J. Mater. Process. Technol., **205**(1–3), pp. 34–41.
[16] Young, H. T., Liao, H. T., and Huang, H. Y., 2006, "Surface Integrity of Silicon Wafers in Ultra Precision Machining," Int. J. Adv. Manuf. Technol., **29**(3–4), pp. 372–378.
[17] Li, H. N., Yu, T. B., Da Zhu, L., and Wang, W. S., 2017, "Analytical Modeling of Grinding-Induced Subsurface Damage in Monocrystalline Silicon," Mater. Des., **130**(Sept.), pp. 250–262.
[18] Yan, J., Asami, T., Harada, H., and Kuriyagawa, T., 2009, "Fundamental Investigation of Subsurface Damage in Single Crystalline Silicon Caused by Diamond Machining," Precis. Eng., **33**(4), pp. 378–386.
[19] Yin, J., Bai, Q., and Zhang, B., 2018, "Methods for Detection of Subsurface Damage: A Review," Chinese J. Mech. Eng., **31**(May), p. 41.
[20] He, S., Zheng, T., and Danyluk, S., 2004, "Analysis and Determination of the Stress-Optic Coefficients of Thin Single Crystal Silicon Samples," J. Appl. Phys., **96**(6), pp. 3103–3109.
[21] Jagailloux, F., Valle, V., Dupré, J.-C., Penot, J.-D., and Chabli, A., 2016, "Applied Photoelasticity for Residual Stress Measurement Inside Crystal Silicon Wafers for Solar Applications," Strain, **52**(4), pp. 355–368.
[22] Geiler, H. D., Wagner, M., Karge, H., Paulsen, M., and Schmolke, R., 2002, "Photoelastic Stress Evaluation and Defect Monitoring in 300-mm-Wafer Manufacturing," Mater. Sci. Semicond. Process., **5**(4–5), pp. 445–455.
[23] Geiler, H. D., Kürner, W., and Storbeck, O., 1999, "Photoelastic Imaging of Process Induced Defects in 300mm-Silicon Wafers," MRS Proc., **591**(Feb.), p. 249.
[24] Skenes, K., Prasath, R. G. R., and Danyluk S., 2014, "Polariscopy Measurement of Residual Stress in Thin Silicon Wafers," *Residual Stress, Thermomechanics & Infrared Imaging, Hybrid Techniques and Inverse Problems*, Vol. 8, M. Rossi, M. Sasso, N. Connesson, R. Singh, A. DeWald, D. Backman, and P. Gloeckner, eds., Springer International Publishing, Cham, pp. 79–85.
[25] Gogotsi, Y., Baek, C., and Kirscht, F., 1999, "Raman Microspectroscopy Study of Processing-Induced Phase Transformations and Residual Stress in Silicon," Semicond. Sci. Technol., **14**(10), p. 936.
[26] Suzuki, T., Nishino, Y., and Yan, J., 2017, "Mechanisms of Material Removal and Subsurface Damage in Fixed-Abrasive Diamond Wire Slicing of Single-Crystalline Silicon," Precis. Eng., **50**(Oct.), pp. 32–43.
[27] Ravindra, D., Ghantasala, M. K., and Patten, J., 2012, "Ductile Mode Material Removal and High-Pressure Phase Transformation in Silicon During Micro-Laser Assisted Machining," Precis. Eng., **36**(2), pp. 364–367.
[28] Bismayer, U., Brinksmeier, E., Güttler, B., Seibt, H., and Menz, C., 1994, "Measurement of Subsurface Damage in Silicon Wafers," Precis. Eng., **16**(2), pp. 139–144.
[29] Balogun, O., Cole, G. D., Huber, R., Chinn, D., Murray, T. W., and Spicer, J. B., 2011, "High-Spatial-Resolution Sub-Surface Imaging Using a Laser-Based Acoustic Microscopy Technique," IEEE Trans. Ultrason. Ferroelectr. Freq. Control., **58**(1), pp. 226–233.
[30] Ishikawa, I., Kanda, H., Katakura, K., and Semba, T., 1989, "Measurement of a Damaged Layer Thickness With Reflection Acoustic Microscope," IEEE Trans. Ultrason. Ferroelectr. Freq. Control., **36**(6), pp. 587–592.
[31] Fine, K. R., Garbe, R., Gip, T., and Nguyen, Q., 2005, "Non-Destructive Real-Time Direct Measurement of Subsurface Damage," Proceedings Volume 5799, Modeling, Simulation, and Verification of Space-based Systems II, Orlando, FL, May 19, pp. 5796–5799.
[32] Bertussi, B., Cormont, P., Palmier, S., Legros, P., and Rullier, J.-L., 2009, "Initiation of Laser-Induced Damage Sites in Fused Silica Optical Components," Opt. Express., **17**(14), pp. 11469–11479.

[33] Lu, W. K., Sun, J. G., and Pei, Z. J., 2006, "Subsurface Damage Measurement in Silicon Wafers With Cross-Polarisation Confocal Microscopy," Int. J. Nanomanuf., **1**(2), pp. 272–282.
[34] Zhang, J. M., and Sun, J. G., 2005, "Quantitative Assessment of Subsurface Damage Depth in Silicon Wafers Based on Optical Transmission Properties," Int. J. Manuf. Technol. Manag., **7**(5/6), pp. 540–552.
[35] Winn, A. J., and Yeomans, J. A., 1996, "A Study of Microhardness Indentation Fracture in Alumina Using Confocal Scanning Laser Microscopy," Philos. Mag. A, **74**(5), pp. 1253–1263.
[36] Zheng, T., and Danyluk, S., 2002, "Study of Stresses in Thin Silicon Wafers With Near-Infraredphase Stepping Photoelasticity," J. Mater. Res., **17**(1), pp. 36–42.
[37] Korkh, Y. V., Burkhanov, A. M., and Rinkevich, A. B., 2009, "Scanning Acoustic Microscope for Visualization of Microflaws in Solids," Russ. J. Nondestruct. Test., **45**(10), pp. 677–684.
[38] Zhang, J. M., Sun, J. G., and Pei, Z. J., 2004, "Optical Transmission Properties of Silicon Wafters: Theoretical Analysis," ASME 2004 International Mechanical Engineering Congress and Exposition, Anaheim, CA, Nov. 13–19, pp. 17–24.
[39] Corby, T. W., and Nickola, W. E., 1997, "Residual Strain Measurement Using Photoelastic Coatings," Opt. Lasers Eng., **27**(1), pp. 111–123.
[40] Zhang, J. M., Sun, J. G., and Pei, Z. J., 2002, "Subsurface Damage Measurement in Silicon Wafers by Laser Scattering," Trans Namri/Sme., **30**, pp. 535–542.
[41] Ramesh, K., 2000, "Fusion of Digital Photoelasticity, Rapid Prototyping and Rapid Tooling Technologies," *Digital Photoelasticity: Advanced Techniques and Applications*, K. Ramesh, ed., Springer, Berlin, pp. 347–367.
[42] Ganapati, V., Schoenfelder, S., Castellanos, S., Oener, S., Koepge, R., Sampson, A., Marcus, M. A., Lai, B., Morhenn, H., Hahn, G., Bagdahn, J., and Buonassisi, T., 2010, "Infrared Birefringence Imaging of Residual Stress and Bulk Defects in Multicrystalline Silicon," J. Appl. Phys., **108**(6), p. 63528.
[43] Gao, S., Kang, R. K., Guo, D. M., and Huang, Q. S., 2010, "Study on the Subsurface Damage Distribution of the Silicon Wafer Ground by Diamond Wheel," Adv. Mater. Res., **142**(Oct.), pp. 126–128.
[44] Zhou, L., Tian, Y. B., Huang, H., Sato, H., and Shimizu, J., 2011, "A Study on the Diamond Grinding of Ultra-Thin Silicon Wafers," Proc. Inst. Mech. Eng. Part B J. Eng. Manuf., **226**(1), pp. 66–75.